University of Huddersfield Repository

Arebi, Lufti, Gu, J., Ball, Andrew and Gu, Fengshou

Investigation of a Rotating Shaft with a Novel Integrated Wireless Accelerometer

Original Citation

Arebi, Lufti, Gu, J., Ball, Andrew and Gu, Fengshou (2010) Investigation of a Rotating Shaft with a Novel Integrated Wireless Accelerometer. In: The Seventh International Conference on Condition Monitoring and Machinery Failure Prevention Technologies, 22-24 June 2010, Ettington Chase, Stratford-upon-Avon, England, UK.

This version is available at http://eprints.hud.ac.uk/id/eprint/8301/

Investigation of a Rotating Shaft with a Novel Integrated Wireless Accelerometer

L. Arebi, J. Gu, A. Ball and F. Gu

University of Huddersfield, Queensgate, Huddersfield HD1 3DH, UK

Abstract

Rotating shafts are the most critical components of rotating machines such as motors, pumps, engines and turbines. Due to their heavy workloads, defects are more likely to develop during operation. There are many techniques used to monitor shaft defects by analysing the vibration of the shaft as well as the instantaneous angular speed (IAS) of the shaft. The signals are measured either using non-contact techniques such as laser-based measurement or indirect measurement such as the vibration on bearing housings. The advancement in low cost and low power Micro Electro Mechanical Systems (MEMS) make it possible to develop an integrated wireless sensor mounted on rotating shafts directly. This can make the fault diagnosis of rotating shafts more effective as it is likely to capture more details of shaft dynamics. This paper presents a novel integrated wireless accelerometer mounted directly on a rotating shaft and demonstrates that it can effectively monitor different degree of misalignments occurring commonly in a shaft system.

Keywords: Wireless Accelerometer, Rotating Shaft, Vibration, Misalignment

1. Introduction

The most common cause of machine vibration is rotor misalignment after imbalance. This vibration is due to reactive forces in the couplings. Understanding and practicing the fundamentals of rotating shaft parameters is the first step in reducing unnecessary vibration, reducing maintenance costs and increasing machine uptime. In industry, 30% of a machine's downtime is due to the poorly aligned machines[1].

Misalignment is estimated to cause over 70% of rotating machinery's vibration problems[3]. Hence, an in-depth study and an accurate knowledge on the vibration characteristics is very helpful in understanding and diagnosing the rotor misalignment to avoid any failures or damages that may arise[2].

There are various factors such as differential thermal growth of machines, asymmetry in applied loads, unequal foundation settlement, etc., which disturb the alignment condition of a machine[2]. Despite the rapid increase in the understanding of rotor dynamics, no satisfactory analysis explains the range of observed phenomena[1]. Vance[4] and Goodman[5] observed that misalignment is present due to improper machine assembly and sometimes, the thermal distortion of the bearing housing supports, resulting in abnormal rotating preload. However, a perfect alignment between the driving and driven shafts cannot be attained. Gibbons[6] first derived the misalignment reaction forces from those generated in different types of couplings.

Xu and Marangoni[7] showed analytically that the vibration due to coupling misalignment mainly occur at the even multiples of the rotor speed. Sekhar and Prabhu[8] numerically evaluated the effect of coupling misalignment on the vibration response of the rotor. They suggested 2X vibration response as a characteristic signature of misaligned shafts. Dewell and Mitchell[11] showed experimentally that 2X and 4X vibration components are largely dependent upon coupling misalignment.

Lee[9] derived a model for the flexible coupling–rotor–ball bearing system, including reaction loads from deformations of rolling elements of bearing and coupling elements as the misalignment effects. From orbital analysis, anisotropy of bearing stiffness was suggested as the misalignment indicator. The other approach often used to simulate misalignment effect in rotor system is from kinematics of the couplings.

Piotrowski[10] concluded that vibration due to misalignment is usually characterized by a 2X running speed component and high axial vibration levels. When a misaligned shaft is supported by rolling-element bearing, these characteristic frequencies may also appear. Tejas and Ashish[2] found from the measured forces that the presence and type of misalignment (parallel and angular misalignment) has significant influences on the harmonic content of the misalignment excitation forces.

From the literature, it is clearly proven that misalignment produces high vibration levels in bearings. It is influenced by the machine speed and the stiffness of the coupling. e.g., rubber couplings are more tolerant and tend to produce less amount of vibration.

Furthermore, the majority of misalignment studies in the past are theoretical; experimental investigations are relatively limited. The theoretical studies are often investigated with simplified assumptions. The outcome of these studies may not be accurate, since in practice there are many more sources of observed vibration characteristics in an actual rotor system. All of these studies used wired accelerometer which is usually attached to the bearings. However, this work presents a novel way to investigate shaft misalignment based on a newly designed wireless accelerometer. As the sensor is mounted directly on the shaft, the true dynamics of the shaft can be recorded. In addition, it focuses specifically on experimental study of misaligned coupled rotors supported by ball and roller bearings.

2. Wireless Sensor Development

The wireless accelerometer node used in this research was developed using a MEMS accelerometer ADXL202AE with a duty cycle output which can be conditioned conveniently to work wirelessly by the transmitter and receiver modules. The accelerometer is able to measure positive and negative absolute accelerations of $\pm 2g$.

The duty cycle period is adjustable from 0.5 ms to 10 ms via a single resistor (R_{SET})[12]. The duty cycle outputs are available from X_{OUT} and Y_{OUT} pins. Moreover, the analogue output can be reconstructed by filtering the duty cycle outputs.

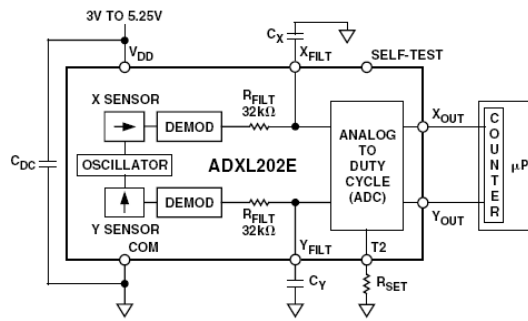The bandwidth of the ADXL202 can be set from 10 Hz to 5 kHz via capacitors C_X and C_Y as shown in Figure 1[12].

Figure 1 Accelerometer block diagram[12]

2.1 Duty Cycle Signal (DCS)

Duty cycle signal depicted in Figure 2 has a period of T and duty cycle D. The value of D finds out the percent of duty cycle of ON time corresponds to the period time T, 100% being fully ON. A low duty cycle is associated with low power due to the power being OFF for most of its time.
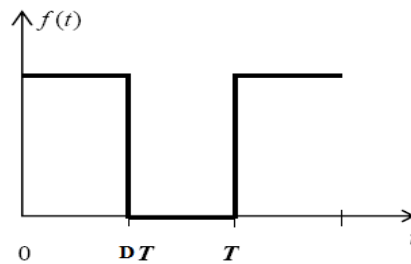

Figure 2 Duty cycle signal with period T and duty cycle D

The DCS resolution is defined as the maximum number of pulses can be fit into a DCS period that means 100%[13]. The DCS period is defined as an arbitrarily time period in which DCS take place. It is chosen to suit a specific application[3].

The easiest and cheapest way to reconstruct the analogue signal from the duty cycle is to use a low-pass filter with a cut-off frequency below the carrier frequency. Ideally, this filter can remove the high frequency harmonics and only leaves the D.C. component. In addition, the filter will allow the duty cycle to vary at frequencies up to the cut-off frequency and reflect this variation with a corresponding voltage level change in the D.C. output. However, a real filter always allows some portion of the harmonics to pass, which produces ripples in the desired output. A trade-off between harmonic ripple and duty cycle carrier frequency is required during the design of an analogue low-pass filter for specific applications.

2.2 Circuit Design

The first step in the design is to select the period of duty cycle (T) so that the analogue output can be reconstructed. According to the specifications of the accelerometer, T should be in the range of from 0.5ms to 0.9ms.

The duty cycle period was adjusted to 0.544ms by the resistor (R_{SET}=68 KΩ). Therefore, the frequency of DCS was 1.838 kHz. The bandwidth of the accelerometer was set to 500 Hz by selecting capacitors C_x and C_y to be 0.01 μF.

2.2.1 Wireless Accelerometer Operating Description

The DCS signal of the Wireless accelerometer is sent by the transmitter module in radio frequency waves at 418MHz, as shown in Figure 3a. This radio frequency signal is acquired by the receiver module shown in Figure 4b and sent to the Sallen-Key low pass filter with cut-off frequency of 131.5Hz to reconstruct the analogue signal. The analogue signal from the low pass filter is outputted to the data acquisition system (DAS). The signal is sampled at 96000Hz by DAS and the recorded data is processed using Matlab.
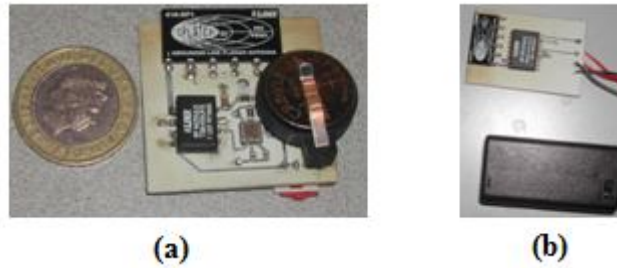

Figure 3 Wireless sensor: (a) Wireless accelerometer node circuit and (b) Receiver circuit

2.2.2 Sensitivity of the Wireless Sensor

The +1g accelerometer's output (A) was measured by pointing the x-axis of wireless accelerometer directly to the earth. The sensor then is turned 180° to measure the output at -1g (B). Using the two duty cycle readings from the oscilloscope, the sensor sensitivity is calculated by[12]:

$$\text{Sensitivity } (S_a) = \frac{A-B}{2g} \tag{1}$$

$$Sensitivity(S_a) = \frac{72.8\% - 54.5\%}{2g} = 9.15\%/g \tag{2}$$

Since the voltage supply V_{DD}=3Volts

$$S_a = 9.15\%/g \times 3V = 274.5mV/g = 27.98165 \ mV/ms^{-2} \tag{3}$$

2.3 Frequency Response

The frequency response of the wireless accelerometer was evaluated by comparing it with a commercial accelerometer with a known frequency response. Figure 4 shows the calibration system which consists of a JZK-2 model shaker (vibrator), a function generator and an amplifier. Two wired accelerometer were used to calibrate the developed wireless accelerometer: One was ADXL202AE, the same type as the wireless

sensor; the other was ADXL322. The three accelerometers, as shown in Figure4, were held by an aluminium rectangular frame and mounted to the vibrator.
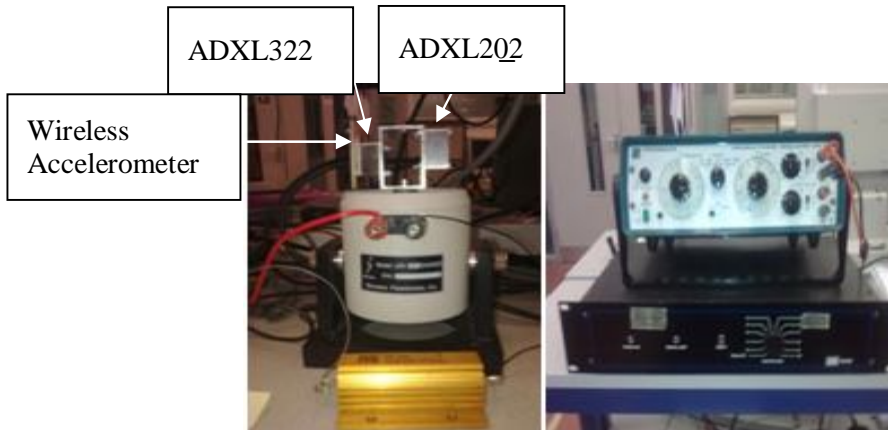

Figure 4 Sensor calibration system using JZK-2 vibrator

The vibrator was driven by the amplified sine wave from the signal generator and amplifier unit. The frequency responses of the accelerometers to every change in the sine waveform frequency were recorded. Throughout this test, the accelerometer's practical resonant frequency was determined and the signal output with respect to different vibration frequencies was examined.
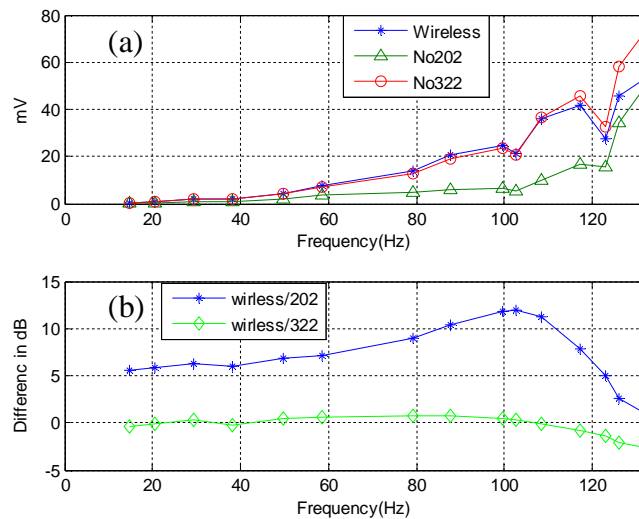

Figure 5 Frequency response comparison between a wireless accelerometer and two wired ones (ADXL202 and ADXL322)

The outputs of accelerometers were recorded using data acquisition with a sampling frequency of 96 kHz and the results were processed using Matlab. Figure 5(a) shows the amplitude frequency response of the three accelerometers. It can be observed that the response of the wireless accelerometer is very close to ADXL322 and notably different from ADXL202. This is because the wireless accelerometer was mounted next to ADXL322 accelerometer while the ADXL202 was mounted on the other side of the

holder, as shown in Figure 4. Although the bandwidth of both wired accelerometers are 500Hz, the wireless accelerometer's bandwidth is limited by the low pass filter, which is 131.5Hz.

3. Test System

The bearing test rig, shown in Figure 6, was employed in this experimental study. It consists of a 3-phase electrical induction motor to provide a prime power source and a DC generator to apply load to the motor. The motor is connected to the generator through two pieces of shafts, which are connected by three pairs of flexible couplings and supported by bearings in two bearing housings. The construction allows the study of different types of misalignments such as angular and parallel misalignments in different parts of the shaft system. The wireless accelerometer was mounted directly on the shaft connecting to the shaft of the motor while an encoder (type RI32) was mounted at the rotor end of the induction motor as shown in Figure 6. The test rig can run in a speed range from 60rpm to 1420rpm.
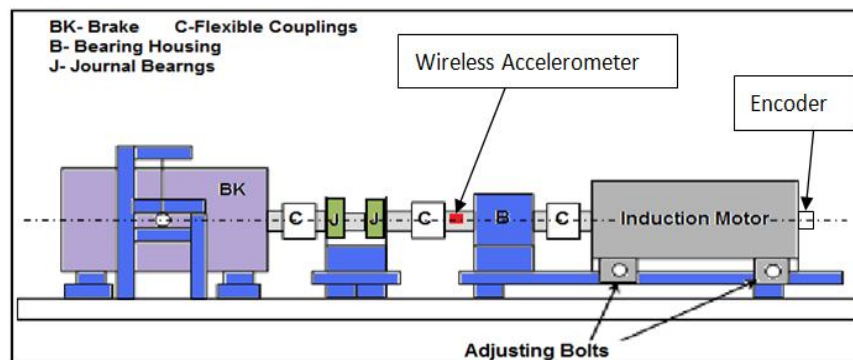

Figure 6 Test rig schematic and wireless sensor placement

4. Test Method

The wireless accelerometer is mounted directly on the second shaft. As depicted in Figure 7. The principal axis of the sensor is along the tangential direction as indicated in the left drawing of Figure 7.
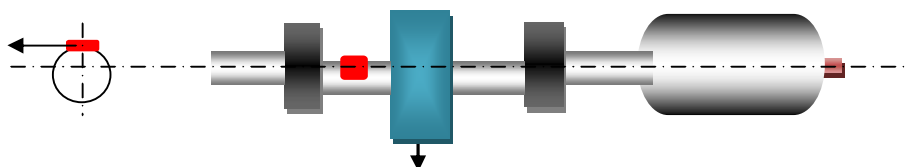

Figure 7 Schematic diagram of misaligned shaft

Figure 8 summarizes the procedure of the test. The test was conducted by comparing the results of IAS signals extracted from the encoder and the acceleration from the wireless accelerometer after each change of the alignment condition. Using the dial indicator, different degrees of misalignment of the second shaft is adjusted to designed values. The couplings installed in this test rig are flexible couplings. The misalignment type used for this test is a parallel misalignment in the horizontal direction.
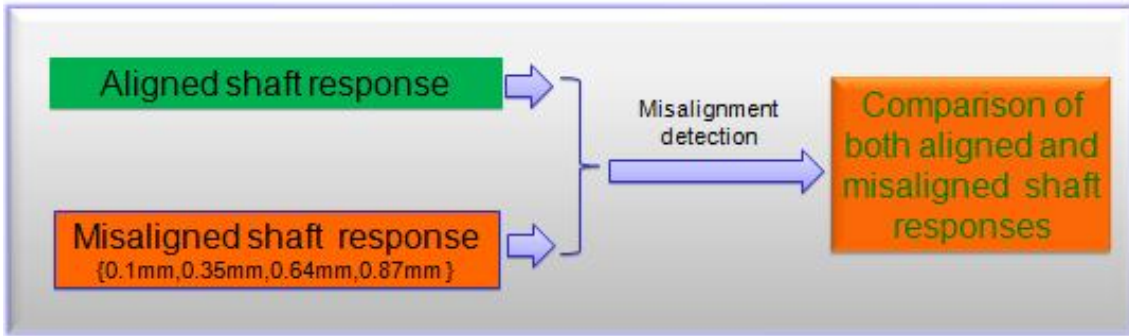
Figure 8: Misalignment test procedure

The steps of the test conducted are:

- Wireless accelerometer is mounted directly on the second shaft.

- The received signal from wireless sensor is fed to a Law Pass Filter (LPF) to reconstruct the analogue form of the signal. The output of LPF is connected to a high performance Data Acquisition System(DAS).

- The signal from encoder is conditioned and also connected to the DAS simultaneously.

- The test rig then ran under different speeds at a fixed load (50%) when it is in healthy condition with minimal misalignment between different shafts. The data was collected from both the wireless accelerometer and the encoder.

- Using a dial indicator, the first misaligned shaft is applied. The test rig then ran for different speeds and the data was collected. This step is repeated for different misalignments.

- The collected data is then analysed using a Matlab program.

While the wireless accelerometer was mounted on the shaft, the receiver, which receives duty cycle signal of the sensor, was connected to Sallen-Key second order active low pass filter with a cut-off frequency of 131.5 Hz. This filter is designed to filter the duty cycle signal in order to reconstruct the analogue form of acceleration signals. Then, the filtered signals are fed to a high speed data acquisition system. The sampling frequency was set to 96kHz to capture more details in the waveform for further analysis. The recorded signals were processed using a program developed in Matlab.

5. Result and Discussion

Figure 9 shows typical waveforms for different misalignments and shaft speeds. As illustrated in the top row of the figure, the outputs of the wireless sensor for healthy case show clear periodic oscillations respective to shaft fundamental period. This may be due to inevitable misalignment from other shafts in the system. In contrast, cases with high degree of misalignments exhibit only a small increase in waveform amplitudes. Nevertheless this small increase can be used to detect the occurrence of misalignments.

To compare waveforms more accurately, the root mean square (RMS) values are calculated over different misalignment cases. As shown in Figure 10, RMS amplitudes are clearly higher at faster speeds and greater misalignments. This demonstrates that RMS values of wireless outputs can be based on to differentiate the high misalignment cases from the healthy case and between different degrees of misalignment.

In addition, Figure 10 also shows that there are several low amplitude points in the trends with respect to different speeds and different degrees of misalignments. Especially, in the low speed and low misalignment cases, the trends behave very irregularly. Obviously this is not consistent with theoretical prediction. To understand this uncertainty, spectrum analysis is carried out.
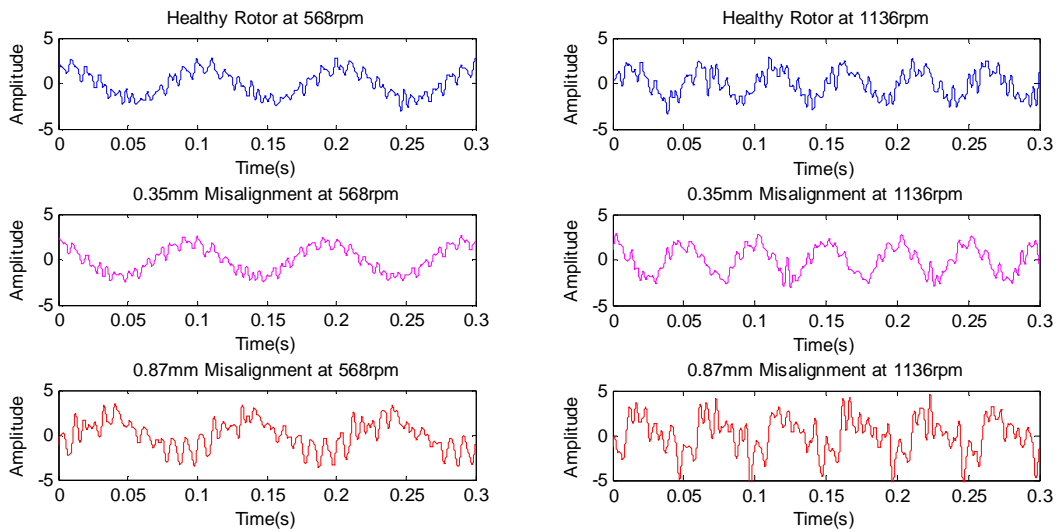

Figure 9 Acceleration waveforms for different shaft conditions at higher and lower speeds

Figure 11 shows typical spectra for the healthy case and the case with the highest misalignment over different speeds. For the healthy case, the shaft frequency is the dominant component and more components in higher order harmonics can be observed at higher speed. For the misalignment case, most of spectral amplitudes become higher and more harmonic components appear as the speed increases.

However, it was found that the shaft frequency produces a modulation to the component at 100Hz. Further investigation show that the 100Hz component is due to the imbalance of power supply between three phases. The interactions between the higher order harmonics of the shaft frequency and the sidebands of 100Hz may lead to irregular fluctuation in the spectral amplitudes over speed and misalignment. In particular, if the two components appear at a same frequency value but their phases are opposite, the amplitude becomes lower. However, the amplitude becomes very high if the two components have the same phases. As shown in Figure 11, all of the irregular amplitudes appear at intersects between the higher order harmonic lines (illustrated by blue dotted lines), and the sideband lines (illustrated by pink dotted lines). Therefore, it can be confirmed that the irregularities in the speed and misalignment trends are due to

the modulation, careful analytical thoughts must be considered for using the amplitude to generate differences between different cases for fault diagnosis.
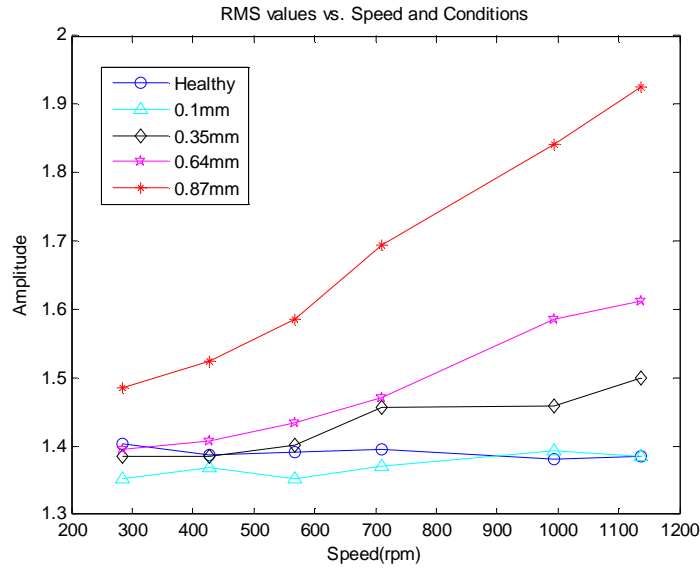

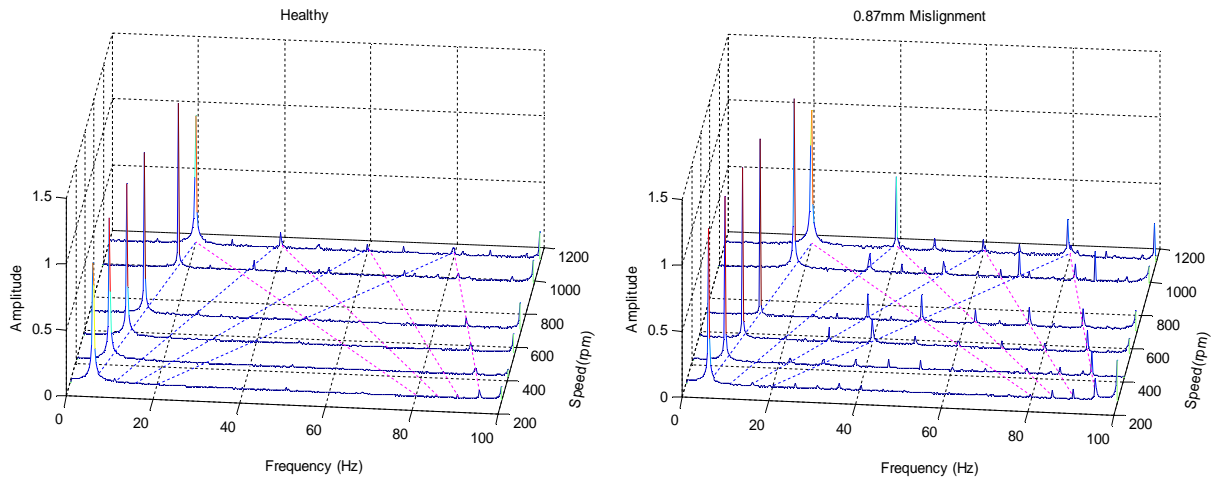Figure 10 Waveform RMS values versus speeds and misalignments.

Figure 11 Spectra versus speed for healthy case

Nevertheless it has been observed from the spectra that amplitudes at shaft frequency under low speeds show a significant difference between the healthy and the misaligned case. The amplitudes for all the test cases are then extracted for detecting low misalignment cases. As shown in Figure 12, misalignment cases below 1000rpm can be separated from the healthy case, proving that the shaft frequency amplitude from the wireless sensor is capable of detecting a fault at low speeds.

However, as shown in Figure 12, using the shaft frequency amplitude alone cannot yield a proper discrimination between different misalignments. In order to compensate for this, perhaps the results in Figure 10 have to be employed. It means that combining the

shaft frequency amplitudes with the RMS values can give both detection and diagnosis results for most of the faulty cases.
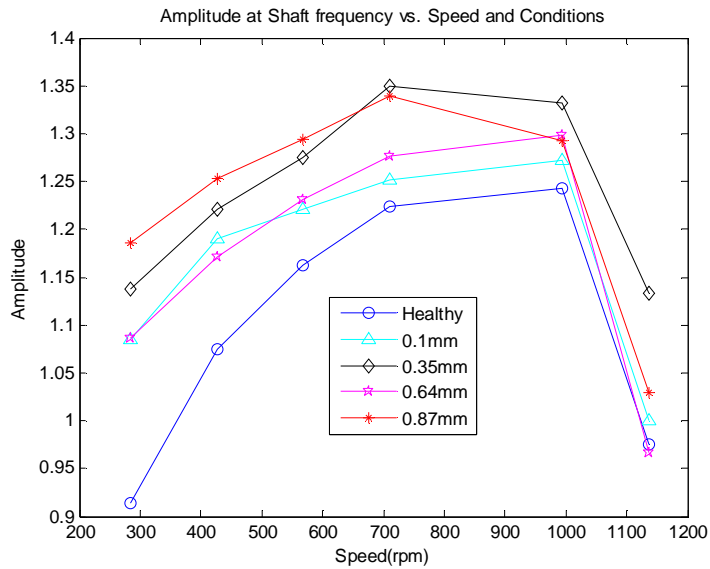

Figure 12 Detection performance based on shaft frequency component

6. Conclusion

Based above analysis, the low cost and low power consumption wireless accelerometer developed in this study can be used to measure the dynamics of a rotating shaft directly. The results in monitoring with the sensor a misaligned shaft show that the frequency amplitudes can separate the healthy case from different degrees of misalignments below 1000rpm. In association with waveform RMS, it can also produce diagnostic results for higher misalignment cases. In addition, it was also found that there is a significant imbalance in the test system. These interim results conclude that the wireless sensor can convey detailed information about the misaligned rotating shaft. Consequently, wireless sensing has unequivocal potential of effective shaft misalignment detection.

References

1. V. Hariharan, PSS. Srinivasan, Kongu Engg, 'Vibration analysis of misaligned shaft –ball bearing system', Indian Journal of Science and Technology, Vol.2 No. 9 (Sep 2009), ISSN: 0974- 6846.

2. TejasH. Patel , AshishK. Darpe, 'Experimental investigations on vibration response of misaligned rotors', Department of Mechanical Engineering, Institute of Technology, India, Mechanical Systems and Signal Processing 23 (2009) 2236–2252.

3. S.R. Bognatz, 'Alignment of critical and non critical machines', Orbit (1995) 23–25.

4. Vance JM (1988) Rotor dynamics of Turbomachinery. New York, John Wiley & Sons.

5. Goodman MJ (1989) Dynamics of rotor – bearing systems. London, Unwin Hyman Ltd.

6. C.B. Gibbons, Coupling misalignment forces, in: Proceedings of the 5th Turbo Machinery Symposium, Gas Turbine Laboratory, Texas A & M University, Texas, 1976, pp. 111–11306.

7. M. Xu, R. Marangoni, 'Vibration analysis of a motor-flexible coupling-rotor system subjected to misalignment and unbalance Part I: Theoretical model and analysis', Journal of Sound and Vibration 176 (1994) 663–679.

8. A.S. Sekhar, B.S. Prabhu, 'Effects of coupling misalignment on vibration of rotating machines', Journal of Sound and Vibration 185 (1995) 655–671.

9. Y.S. Lee, C.W. Lee, 'Modelling and analysis of misaligned rotor–ball bearing systems', Journal of Sound and Vibration 224 (1999) 17–32.

10. J. Piotrowski, 'Shaft Alignment Handbook', Marcel Dekker Inc., New York, 1995.

11. Dewell DL and Mitchell LD (1984), 'Detection of a misaligned disk coupling using spectrum analysis'. ASME Trans. J. Vibration, Acoustics, Stress & Reliability Design. 106, 9-16.

12. Analog Devices, Inc, ADXL202E Catalogue, at http://www.analog.com, 2000.

13. David M. Alter, 'Using PWM Output as a Digital-to-Analog Converter on a TMS320F280x Digital Signal Controller, DSP Applications-Semiconductor Group', Texas Instruments, SPRAA88A – September 2008.